World Journal of Advanced Research and Reviews
eISSN: 2581-9615 CODEN (USA): WJARAI
Cross Ref DOI: 10.30574/wjarr
Journal homepage: https://wjarr.com/

(RESEARCH ARTICLE)

Check for updates

Piezoelectric energy harvesting from a dump truck suspension system

Drissa Mohamed Malo * and Erol Uzal

Department of Mechanical Engineering, İstanbul Üniversitesi - Cerrahpaşa, Istanbul, Turkey.

World Journal of Advanced Research and Reviews, 2022, 15(02), 099–113

Publication history: Received on 25 June 2022; revised on 01 August 2022; accepted on 03 August 2022

Article DOI: https://doi.org/10.30574/wjarr.2022.15.2.0769

Abstract

The suspension system is an important component of a truck. It provides stability to the vehicle, maneuverability, and comfort. A lot of energy is dissipated through this system. In order to scavenge this dissipated energy, piezoelectric stacks can be installed in the system. One of the factors which significantly impacts the harvested power voltage is the location and connection type of the piezoelectric stack in the suspension system. The series connection between the suspension spring and the piezoelectric material has been preferred in this study for it will not affect the mechanical properties and performances of the system. The equivalent system stiffness is increased and the ride comfort is negatively affected in case of a parallel connection between the suspension spring and the piezoelectric stack. The equations of motion of the truck were derived. Harmonic excitation simulations have been run in the MATLAB Simulink software in order to assess the potential of the energy harvesting from truck suspension systems through piezoelectric stacks.

Keywords: Mathematical modeling; Piezoelectric ceramics; Vehicle suspension system; Energy harvesting; Energy dissipation

1. Introduction

All means of transport which consume petroleum products cause environmental pollution during burning and refueling cycles [1]. In 2019, a report from the Energy Information Administration (EIA) [2] revealed that 91% of the total energy demands of the US transportation sector were met by petroleum-based fuels. However, only a small amount of this energy is utilized by the vehicle to move [3, 4]. The suspension system is a key component of trucks as they support the weight and provide ride quality and comfort by absorbing road inconsistencies [5]. Despite this importance, it is one of the main sources of energy loss through vibration dampening. According to Velinsky and White [6], the amount of energy dissipated depends on several parameters such as the vehicle's speed, mass, spring stiffness, damping coefficients, and road profile.

Indeed, the increase of the mass of the vehicle combined with an augmentation of the damping and stiffness coefficient leads to higher energy dissipation in the suspension system as observed in reference [7]. Moreover, the road condition influences the quantity of energy that vanishes through the dampers. The road profile can be analyzed both macrostructurally (longitudinal road profile) and microstructurally (transversal road profile) [8]. The former is designated at a vehicle speed between 25 – 120 km/h while the latter represents the shocks sensed by the passengers due to the bumps. It was noticed that the microstructural profile has the most important effect on the VSS. Wei and Taghavifa in their works [9] highlighted 04 categories of road surfaces in the random excitation configuration. This classification was made based on the power spectral density (PSD) function. These road categories are rough runway, smooth runway, smooth highway, and gravel highway. A significant difference in power dissipation was observed between the smooth and gravel highway configurations (respectively 200W and 2000W). This huge gap can be

* Corresponding author: Drissa Mohamed Malo
Department of Mechanical Engineering, Istanbul University, Cerrapaşa, Istanbul, Turkey.

explained by the variation of the suspension system velocity for the smooth (0.75m/s) and gravel (2m/s) roads. According to the same research work, the suspension system of a car that is subjected to harmonic excitation experiences notably lower power dissipation. Indeed, an average power loss of 57.84 W was reported at the speed of 13 km/h and 39 km/h. Abdel Kareem et al. [10] revealed that at a speed of 20 -50 km/h, the power dissipated by conventional dampers on a flat road is in a range of 10 – 90W against 40 – 140W for a road with no less than one bump. The findings of the aforementioned works stipulate that the energy wasted through mechanical vibrations is non-negligible. Consequently, the main goal of this work is to assess the potential VSS energy harvesting to turn vibrations into useful electrical energy.

Aljadiri et al. mentioned in their research work [11] the benefits and limitations of the different vibration-based energy harvesting techniques. Electromagnetic transducers have the ability to function without any extra voltage input and are not subjected to any mechanical constraints. Furthermore, they can supply high output current. In contrast, they offer a low voltage output and display poor performances when they are used in microstructural applications. In addition to that, they are difficult to integrate with Micro-Electro-Mechanical Systems (MEMS) fabrication procedures. In comparison, electrostatic transducers can be easily integrated with MEMS fabrication procedures and can provide a high voltage output. Nevertheless, they display drawbacks such as the presence of mechanical constraints, the need for external voltage input, and their low output current. It can be noticed in Table 1 that piezoelectric generators offer the most advantages such as their simplicity, ability to work without any external voltage input, wide frequency range, and ease of use in diverse applications.

Energy harvested through piezoelectric transduction can be used in various applications such as wireless sensors, lighting and battery charging, and so on [12]. Thanks to their decreasing costs, their increased sensitivity, and the advances in radio frequency technology, the use of sensors in agriculture have been popularized in the last few years [13]. For instance, sensors can be installed in greenhouses, on farming machinery, in the fields, or on livestock. The use of wireless sensors use in agri-food allows data collection and condition monitoring in tough environments increasing farmers' productivity. Ipema et al [14], Nadimi et al [15] used wireless technology to monitor cows and collect data such as animal presence, pasture time, and body temperature measurements. The use of remote wireless sensors was developed in the industrial sector to support industrial automation and meet the ever-increasing demand.

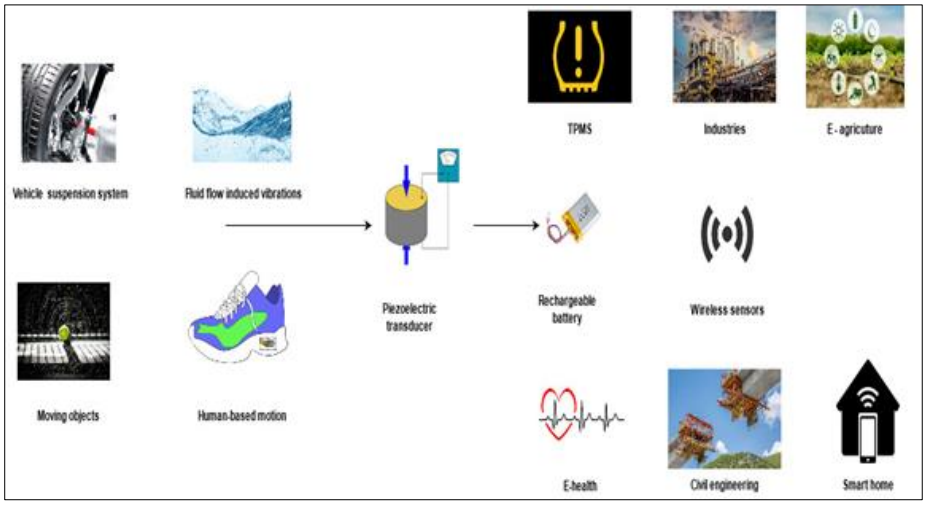

Figure 1 Piezoelectric energy harvesting and its main applications [22-31]

Chen et al. performed research work [16] on the integration of control systems with wireless sensors and actuators networks. An innovative, collaborative, and distributed estimation approach was proposed. The results indicated that the control objectives were achieved. Christin et al. conducted a survey [17] on the challenges faced by the acceptance of wireless sensors used in industrial applications. The outcomes of the evaluation enabled the identification and discussion of open issues. The popularization of sensors also provided the medical sector with a revolution in the domain of remote patient monitoring.

Ko et al. reviewed in their work [18] the main applications of wireless sensor networks in the healthcare sector. Key challenges related to the privacy and security of personal data were discussed. They also highlighted the fact that these challenges are worsened by the lack of resources. Prototype systems for physiological and behavioral monitoring were

defined as well as current research works challenges. Furthermore, the use of sensors has experienced a boom in military and civil applications.

García-Hernández et al. [19] carried out a survey on wireless sensor networks and their applications. Their low cost and flexibility allow us to find out innovative and new application areas for remote sensing. Bridges stayed cables are vital for the structural integrity of bridges and their tension was monitored using polyvinylidene difluoride (PVDF) films as sensors as reported in this reference [20]. Chalard et al. in their research work [21] investigated the challenges and encouraging applications of wireless sensor devices. Figure 1. illustrates piezoelectric energy harvesting and its main applications.

Table 1 Conversion mechanisms benefits and limitations [11]

Transduction type	**Piezoelectric**	**Electromagnetic**	**Electrostatic**
MEMS compatibility	Compatible	non-compatible	Compatible
Frequency range	wide	Narrow	Narrow
Mechanical constraints	not needed	not needed	Needed
External voltage	not needed	not needed	Needed
Output current	low	High	Low

2. Material and methods

2.1. Piezoelectric and Truck Parameters

Table 2 Piezoelectric stack properties

Property	**Value**	**Unit**	**Symbol**
Piezoelectric constant	600	pm/V (10^{-12}m/V)	d_{33}
Elastic constant	50	GPa	E_{33}
Dielectric constant	30.975	nF/m	ε_{33}
Front and rear piezoelectric stack mass	1300	g	M_{pf}, M_{pr}
Density	7.8	g/cm^3	ρ
Force factor	30000	N/V	α
Electromechanical coupling coefficient	0,65	N/A	K
Capacitance	4,5	μF	C_p
Front and rear piezoelectric stack stiffness	51	MN/m	K_{pf}, K_{pr}
Internal resistance	20	kΩ	R_p

Table 3 777F Off-highway mining dump truck parameters

Parameter	**Value**	**Unit**	**Symbol**
Half sprung mass (Car body)	45000	Kg	Ms
Front and rear unsprung mass (tire)	3500	kg	Muf, Mur
Front and rear suspension spring stiffness	2300000	N/m	Ksf, Ksr
Front and rear tire stiffness	11000000	N/m	Kuf, Kur
Front and rear suspension damping coefficient	46000	Ns/m	bsf, bsr
Front and rear tire damping coefficient	26573	Ns/m	bus, bur

The piezoelectric stack and truck parameters that will have been used in these simulations are represented in Table 2 and Table 3, respectively. The simulation software used in MATLAB Simulink.

2.2. Quarter Car Model (QCM) without the piezoelectric stack

The quarter car model without the piezoelectric stack is presented in Figure 2. The equation derived from this representation is below:

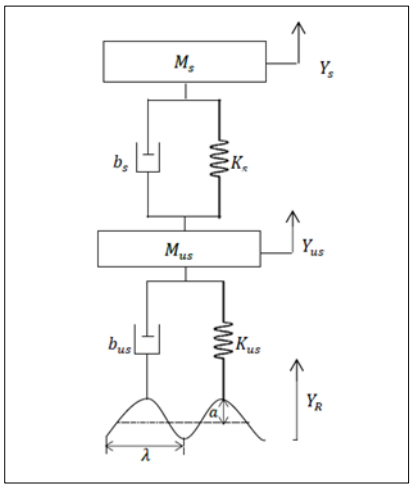

Figure 1 Quarter car model schematic diagram

Equation of vertical motion of the sprung mass:

$$M_s\ddot{y}_s = -K_s(y_s - y_{us}) - b_s(\dot{y}_s - \dot{y}_{us}) \quad \ldots\ldots\ldots\ldots\ldots\ldots\ldots\ldots (1)$$

Equation of vertical motion of the unsprung mass:

$$M_{us}\ddot{y}_{us} = K_s(y_s - y_{us}) + b_s(\dot{y}_s - \dot{y}_{us}) - K_{us}(y_{us} - y_R) - b_{us}(\dot{y}_{us} - \dot{y}_R) \quad \ldots\ldots\ldots\ldots\ldots\ldots\ldots\ldots (2)$$

Where $\dot{y}_R$ is the velocity of the road
$\dot{y}_{us}$ is the velocity of the unsprung mass
$\dot{y}_s$ is the velocity of the sprung mass,
$\ddot{y}_{us}$ is the acceleration of the unsprung mass
$\ddot{y}_s$ is the acceleration of the sprung mass

2.3. Half Car Model (HCM) without the piezoelectric stack

The half-car model without the piezoelectric stack is presented in Figure 3. The equation derived from this representation is below:

Four equations of motions can be derived from the four degrees of freedom of the half car model:

Equation of vertical motion of the front unsprung mass:

$$M_{uf}\ddot{y}_{uf} = K_{uf}(y_{uf} - y_{Rf}) - b_{uf}(\dot{y}_{uf} - \dot{y}_{Rf}) + K_{sf}(y_s - L_f\theta_s - y_{uf}) + b_{sf}(\dot{y}_s - L_f\dot{\theta}_s - \dot{y}_{uf}) \quad \ldots\ldots\ldots\ldots\ldots\ldots\ldots\ldots (3)$$

Equation of vertical motion of the front unsprung mass:

$$M_{ur}\ddot{y}_{ur} = K_{ur}(y_{ur} - y_{Rr}) - b_{ur}(\dot{y}_{ur} - \dot{y}_{Rr}) + K_{sr}(y_s + L_r\theta_s - y_{ur}) + b_{sr}(\dot{y}_s - L_r\dot{\theta}_s - \dot{y}_{ur}) \quad \ldots\ldots\ldots\ldots\ldots\ldots\ldots\ldots (4)$$

Equation of angular motion of the sprung mass:

$$I_s\ddot{\theta}_s = L_f\left[K_{sf}\left(y_s - L_f\theta_s - y_{uf}\right) + b_{sf}\left(\dot{y}_s - L_f\dot{\theta}_s - \dot{y}_{uf}\right)\right] - L_r\left[K_{sr}(y_s + L_r\theta_s - y_{ur}) + b_{sr}\left(\dot{y}_s + L_r\dot{\theta}_s - \dot{y}_{ur}\right)\right]\ldots\ldots\ldots\ldots\ldots(5)$$

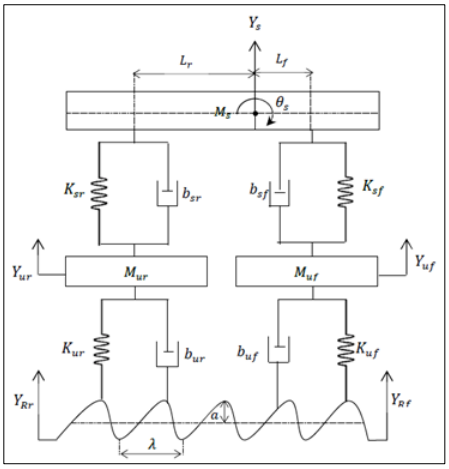

Figure 3 Half car model schematic diagram

Equation of vertical motion of the sprung mass:

$$M_s\ddot{y}_s = -K_{sf}\left(y_s - L_f\theta_s - y_{uf}\right) - b_{sf}\left(\dot{y}_s - L_f\dot{\theta}_s - \dot{y}_{uf}\right) - K_{sr}(y_s + L_r\theta_s - y_{ur}) - b_{sr}\left(\dot{y}_s + L_r\dot{\theta}_s - \dot{y}_{ur}\right)\ldots\ldots\ldots (6)$$

Where: θ_s represents the angular displacement (rad),
I_s Represents the moment of inertia (kg.m^2)
L_f Represents the front wheelbase (m),
L_r Represents the rear wheelbase (m),
$\ddot{y}_{uf}$ Represents the vertical acceleration of the front unsprung mass (front tire),
$\ddot{y}_{ur}$ Represents the vertical acceleration of the rear unsprung mass (rear tire),
$\ddot{y}_s$ Represents the acceleration of the sprung mass (car body),
$\dot{\theta}_s$ Represents the angular velocity of the sprung mass,
$\dot{y}_{uf}$ Represents the vertical velocity of the front unsprung mass,
$\dot{y}_{ur}$ Represents the vertical velocity of the rear unsprung mass,
$\dot{y}_{Rf}$ Represents the vertical velocity of the road at the front of the car,
$\dot{y}_{Rr}$ Represents the vertical velocity of the road at the back of the car.

2.4. Quarter Car Model with the piezoelectric stack

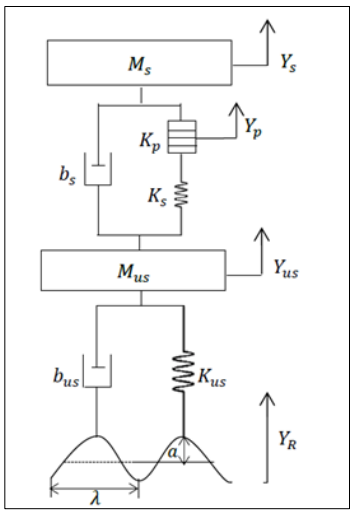

Figure 4 Quarter car model with the piezoelectric stack

The quarter car model with the piezoelectric stack is presented in Figure 4. The equation derived from this representation is below as well as their Laplace transforms.

Equation of vertical motion of the sprung mass:

$$M_s\ddot{y}_s = -b_s(\dot{y}_s - \dot{y}_{us}) - K_p(y_s - y_p) - \alpha v_p \quad \ldots\ldots (7)$$

$$\leftrightarrow [M_s s^2 + b_s s + K_p]Y_s = (b_s s)Y_{us} + (K_p)Y_p - (\alpha)V_p \quad \ldots\ldots (8)$$

Equation of vertical motion of the unsprung mass:

$$M_{us}\ddot{y}_{us} = -K_{us}(y_{us} - y_R) - b_{us}(\dot{y}_{us} - \dot{y}_R) + K_s(y_p - y_{us}) + b_s(\dot{y}_s - \dot{y}_{us}) \quad \ldots\ldots (9)$$

$$\leftrightarrow [M_{us}s^2 + (b_{us} + b_s)s + (K_{us} + K_s)]Y_{us} = (b_{us}s + K_{us})Y_R + (b_s s)Y_s + (K_s)Y_p \quad \ldots\ldots (10)$$

Equation of the piezoelectric element:

$$M_p\ddot{y}_p = -K_s(y_p - y_{us}) + K_p(y_s - y_p) + \alpha v_p \quad \ldots\ldots (11)$$

$$\leftrightarrow [M_p s^2 + K_s + K_p]Y_p = (K_s)Y_{us} + (K_p)Y_s + (\alpha)V_p \quad \ldots\ldots (12)$$

The equivalent electric system's governing equation (3.18) can be rewritten as:

$$v = \alpha R(\dot{y}_s - \dot{y}_p) - CR\dot{v} \quad \ldots\ldots (13)$$

$$\leftrightarrow (CRs + 1)V = (\alpha Rs)Y_s - (\alpha Rs)Y_p \quad \ldots\ldots (14)$$

The harvested power can be expressed as:

$$P = \frac{V^2}{R} \quad \ldots\ldots (15)$$

2.5. Half Car Model with the piezoelectric stack

The half-car model with the piezoelectric stack is presented in Figure 5. The equation derived from this representation is below:

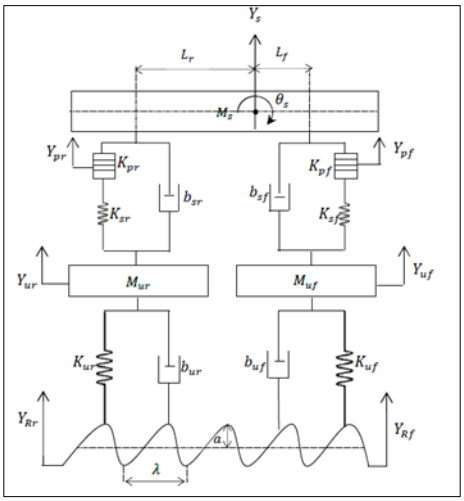

Figure 5 Half car model with the piezoelectric stack

Equation of vertical motion of the front unsprung mass:

$$M_{uf}\ddot{y}_{uf} = -b_{uf}(\dot{y}_{uf} - \dot{y}_{Rf}) - K_{uf}(y_{uf} - y_{Rf}) + b_{sf}(\dot{y}_s - L_f\dot{\theta}_s - \dot{y}_{uf}) + K_{sf}(y_{pf} - y_{uf}) \quad (16)$$

$$\leftrightarrow[M_{uf}s^2 + (b_{sf} + b_{uf})s + (K_{sf} + K_{uf})]Y_{uf} = (b_{uf}s + K_{uf})Y_{Rf} + (b_{sf}s)Y_s - (b_{sf}L_fs)\Theta_s + (K_{sf})Y_{pf} \quad (17)$$

Equation of vertical motion of the rear unsprung mass:

$$M_{ur}\ddot{y}_{ur} = -b_{ur}(\dot{y}_{ur} - \dot{y}_{Rr}) - K_{ur}(y_{ur} - y_{Rr}) + b_{sr}(\dot{y}_s + L_r\dot{\theta}_s - \dot{y}_{ur}) + K_{sr}(y_{pr} - y_{ur}) \quad (18)$$

$$\leftrightarrow[M_{ur}s^2 + (b_{sr} + b_{ur})s + (K_{sr} + K_{ur})]Y_{ur} = (b_{ur}s + K_{ur})Y_{Rr} + (b_{sr}s)Y_s + (b_{sr}L_rs)\Theta_s + (K_{sr})Y_{pr} \quad (19)$$

Equation of vertical motion of the half-sprung mass:

$$M_s\ddot{y}_s = -b_{sf}(\dot{y}_s - L_f\dot{\theta}_s - \dot{y}_{uf}) - b_{sr}(\dot{y}_s + L_r\dot{\theta}_s - \dot{y}_{ur}) - K_{pf}(y_s - L_f\theta_s - y_{pf}) - K_{pr}(y_s + L_r\theta_s - y_{pr}) - (\alpha)v_{pf} - (\alpha)v_{pr} \quad (20)$$

$$\leftrightarrow[M_ss^2 + (b_{sf} + b_{sr})s + (K_{pf} + K_{pr})]Y_s[(b_{sf}L_f - b_{sr}L_r)s + (k_{pf}L_f - K_{pr}L_r)]\Theta_s + (b_{sf}s)Y_{uf} + (b_{sr}s)Y_{ur} + (K_{pf}s)Y_{pf} + (K_{pr}s)Y_{pr} - (\alpha)V_{pf} - (\alpha)V_{pr} \quad (21)$$

Equation of angular motion of the half-sprung mass

$$I_s\ddot{\theta}_s = L_f(b_{sf}(\dot{y}_s - L_f\dot{\theta}_s - \dot{y}_{uf}) + K_{pf}(y_s - L_f\theta_s - y_{pf}) + \alpha v_{pf}) - L_r(b_{sr}(\dot{y}_s + L_r\dot{\theta}_s - \dot{y}_{ur}) + K_{pr}(y_s + L_r\theta_s - y_{pr}) + \alpha v_{pr}) \quad (22)$$

$$\leftrightarrow[I_ss^2 + (b_{sf}L_f^2 + b_{sr}L_r^2)s + (K_{pf}L_f^2 + K_{pr}L_r^2)]\Theta_s = [(b_{sf}L_f - b_{sr}L_r)s + (k_{pf}L_f - K_{pr}L_r)]Y_s - (b_{sf}L_fs)Y_{uf} + (b_{sr}L_rs)Y_{ur} - (K_{pf}L_fs)Y_{pf} + (K_{pr}L_rs)Y_{pr} + (\alpha L_f)V_{pf} - (\alpha L_r)V_{pr} \quad (23)$$

Equation of the rear piezoelectric stack

$$M_{pr}\ddot{y}_{pr} = -K_{sr}(y_{pr} - y_{ur}) + K_{pr}(y_s + L_r\theta_s - y_{pr}) + (\alpha)v_{pr} \quad (24)$$

$$\leftrightarrow[M_{pr}s^2 + (K_{sr} + K_{pr})]Y_{pr} = (K_{sr})Y_{ur} + (K_{pr})Y_s + (k_{pr}L_r)\Theta_s + (\alpha)V_{pr} \quad (25)$$

Equation of the front piezoelectric stack

$$M_{pf}\ddot{y}_{pf} = -K_{sf}(y_{pf} - y_{uf}) + K_{pf}(y_s - L_f\theta_s - y_{pf}) + (\alpha)V_{pf} \quad (26)$$

$$\leftrightarrow [M_{pf}s^2 + (K_{sf} + K_{pf})]Y_{pf} = (K_{sf})Y_{uf} + (K_{pf})Y_s + (k_{pf}L_f)\Theta_s + (\alpha)V_{pf} \quad (27)$$

The constitutive equation of the rear suspension's equivalent electric system can be deduced:

$$v_r = \alpha R(\dot{y}_s + L_r\dot{\theta}_s - \dot{y}_{pf}) - CR\dot{v}_r \quad (28)$$

Similarly, the constitutive equation of the front suspension equivalent electric system can be deduced:

$$v_f = \alpha R(\dot{y}_s - L_f\dot{\theta}_s - \dot{y}_{pf}) - CR\dot{v}_f \quad (29)$$

$$P_r = \frac{V_r^2}{R} \quad (30)$$

$$P_f = \frac{V_f^2}{R} \quad (31)$$

3. Results and discussion

3.1. Bode Magnitude Plots Of The QCM And HCM

The bode plot represents the frequency response of a system in several disciplines such as control theory and stability analysis. A bode plot generally consists of a magnitude and a phase plot. It provides relevant information such as the natural frequencies of the system.

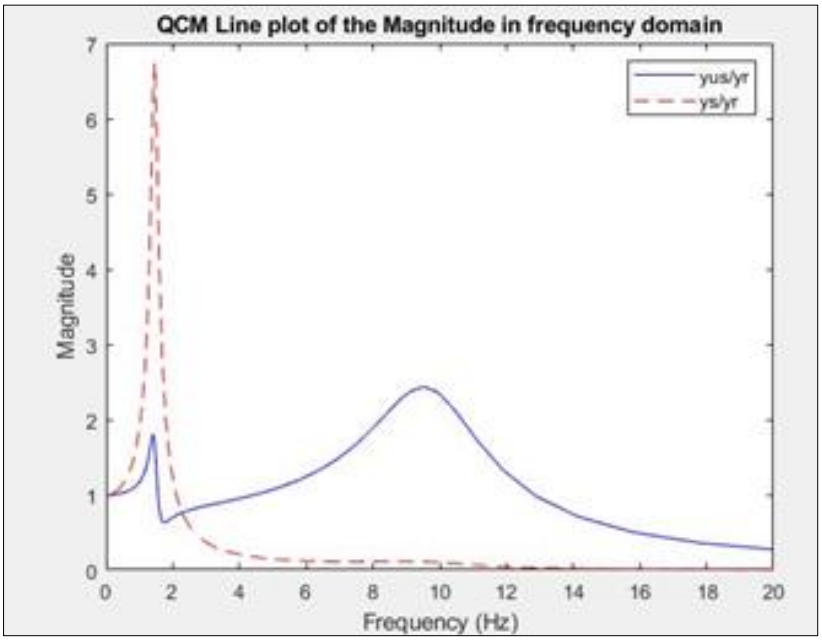

Figure 6 Bode magnitude plot of the QCM

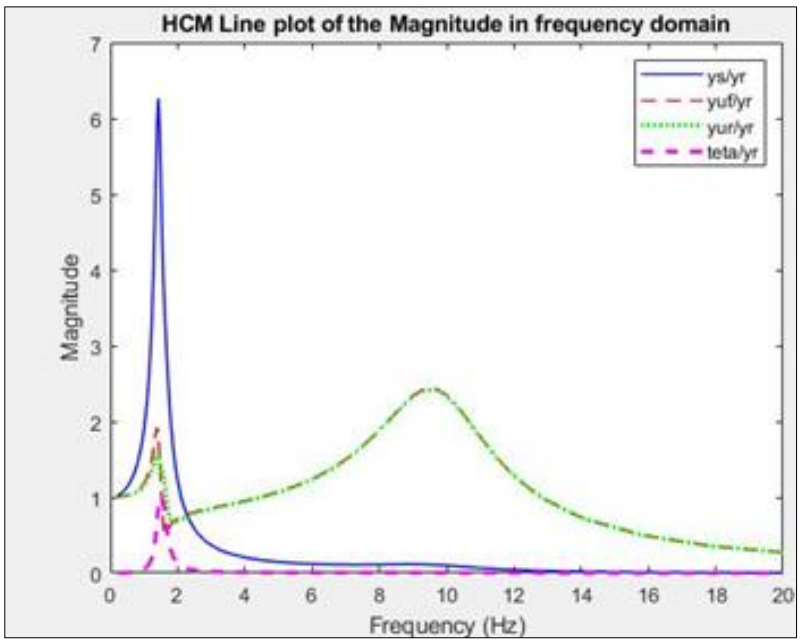

Figure 7 Bode magnitude plot of the HCM

The Bode plot of the QCM is depicted in Figure 6. The natural frequencies are represented in Table 4.

Table 4 QCM natural frequencies

QCM	Frequency (Hz)	harvested voltage plot Peak value (V)	harvested power plot peak value (W)
sprung natural frequency	1.454	20.63	0.02129
unsprung natural frequency	9.529	9.606	0.004614

The Bode plot of the HCM is depicted in Figure 7. Its natural frequencies are represented in Table 5.

Table 5 HCM natural frequencies

HCM	Frequency (Hz)	Front harvested voltage plot Peak value (V)	Front harvested power plot peak value (W)
sprung resonant frequency	1.429	24.26	0.02943
sprung pitch resonant frequency	1.004	3.138	0.004562
Front unsprung resonant frequency	9.66	9.564	0.0004923
Rear unsprung resonant frequency	9.66	9.564	0.004562

3.2. Power Dissipated from QCM And HCM in the Frequency and Velocity Domains

The potential power that can be harvested from the suspension systems is the power dissipated by the suspensions [8]. The power dissipated by the suspension system can be expressed as the product of the relative velocity and their damping force:

$$P_{disQCM} = \frac{b_s\omega^2(y_s-y_{us})^2}{2} \quad \text{..... (32)}$$

$$P_{disHCM} = \frac{b_{sf}\omega^2(y_s-L_f\theta-y_{uf})^2}{2} + \frac{b_{sr}\omega^2(y_s+L_r\theta-y_{ur})^2}{2} \quad \text{..... (33)}$$

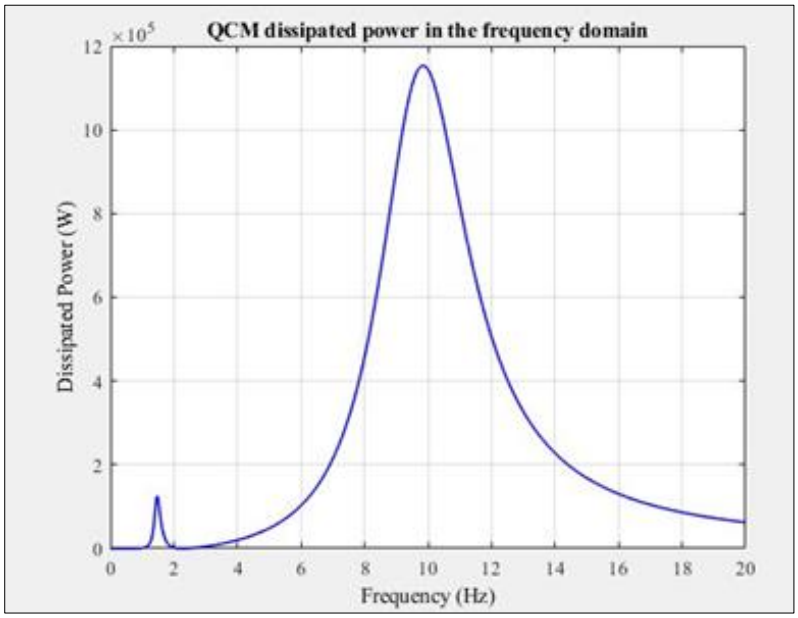

Figure 8 Dissipated power from the QCM suspension in the frequency domain

The power dissipated from the QCM in the frequency and car velocity domains are represented in Figure 8 and Figure 9, respectively. At the sprung natural frequency (1.454 Hz) the dissipated power is $1.233 .10_5$ W and at the unsprung natural frequency (9.529 Hz) its value is $1.112 .10^6$ W.

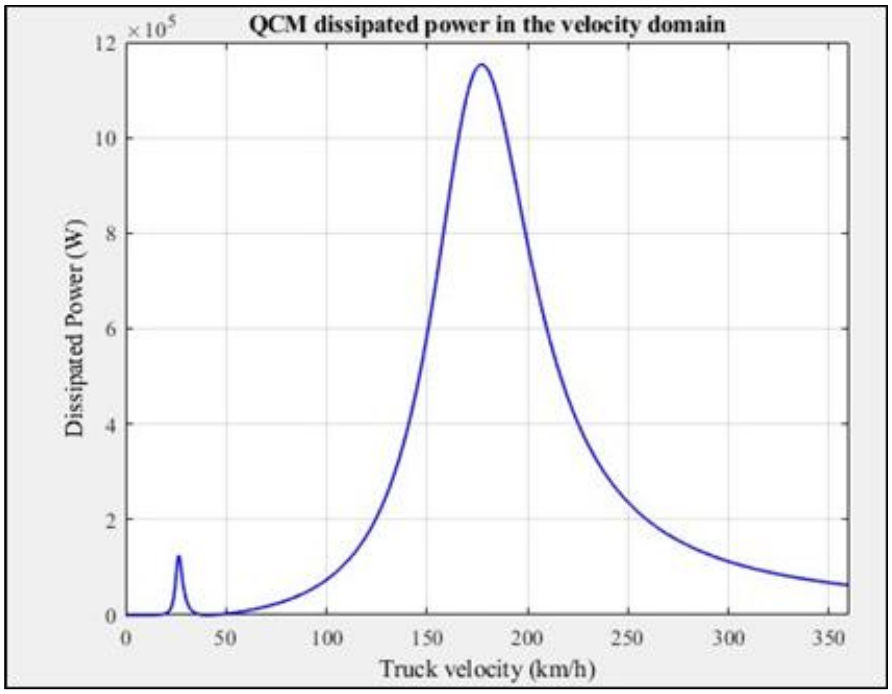

Figure 9 Dissipated power from the QCM suspension according to the truck velocity

The power dissipated from the HCM in the frequency and car velocity domains are represented in Figure 10 and Figure 11, respectively. At the sprung pitch natural frequency (1.004 Hz), the dissipated power is 3695 W. At the sprung natural frequency (1.429Hz) its value is $2.495.10^5$ W. At the unsprung natural frequencies, the dissipated power is $2.274.10^5$ W.

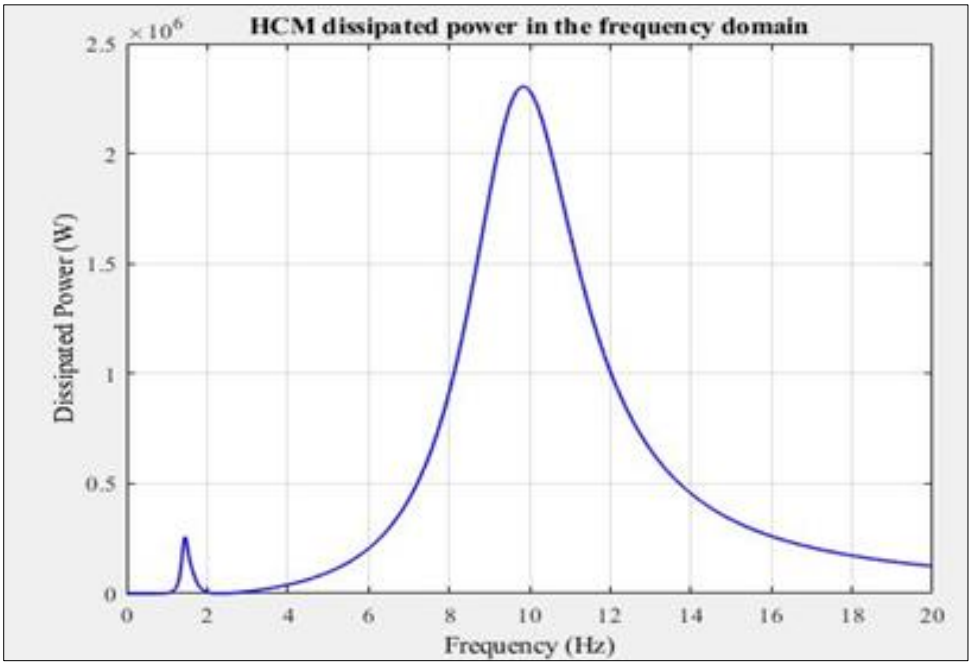

Figure 10 Dissipated power from the HCM suspension in the frequency domain

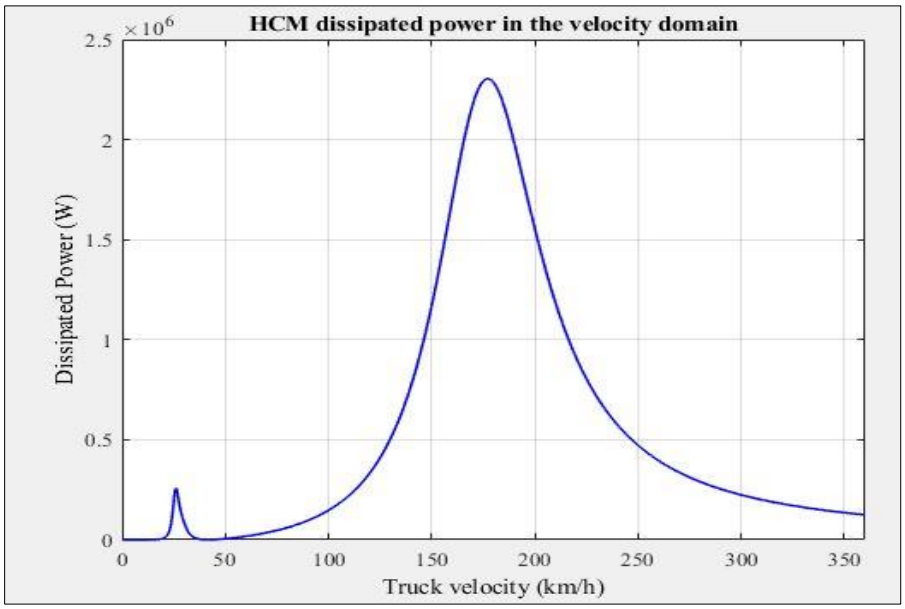

Figure 11 Dissipated power from the HCM suspension according to the truck velocity

3.3. Voltage and Power Harvested from the QCM and HCM in Harmonic Excitations

An approximation of the harmonic excitation of the front and rear tires of the car are given by the following delayed function:

$$y_{Rf} = \text{asin}(\omega t) \quad \text{..... (34)}$$

$$y_{Rr}(t) = y_{Rf}(t - \tau) \quad \text{..... (35)}$$

Where, ω is the angular frequency (is the sprung resonant frequency in both QCM and HCM cases),
a is the acceleration amplitude (assumed to be 0.05m in this study),
τ is the time delay which is equal to $\frac{L}{u}$ where L is the wheelbase and u is the velocity of the truck.

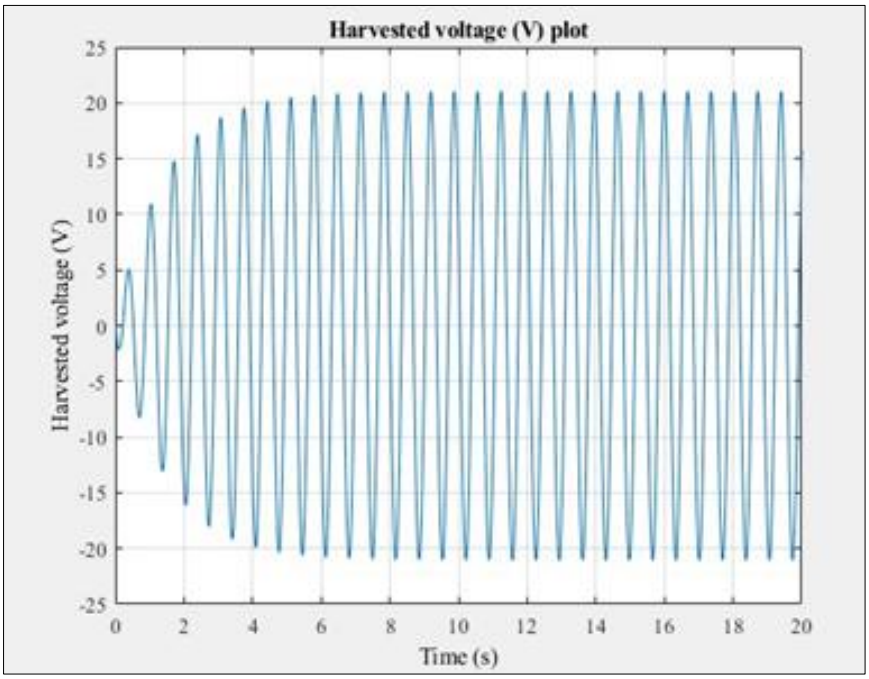

Figure 12 QCM harmonic excitation harvested voltage plot

The voltage and power harvested from the QCM are represented in Figure 12 and Figure 13, respectively. For excitation at the sprung natural frequency, the QCM, the maximum recorded harvested voltage is 20.63V while the maximum harvested power is 0.02129 W. The root-mean-square value of the voltage was obtained by dividing the peak value of the voltage by $\sqrt{2}$. The RMS voltage and power are 14.59V and 0.0007294, respectively.

The voltage and power harvested from the HCM are represented in Figure 14 and Figure 15, respectively. By applying a harmonic excitation to the HCM at the sprung natural frequency the maximum harvested voltage is 24.83 V while the maximum harvested power is 0.03082. The root-mean-square value of the voltage was calculated by dividing it by $\sqrt{2}$. The RMS voltage and power are 17.56 V and 0.0008779 W, respectively. There is an increase of 20.36% in the RMS voltage and power values in comparison with the QCM.

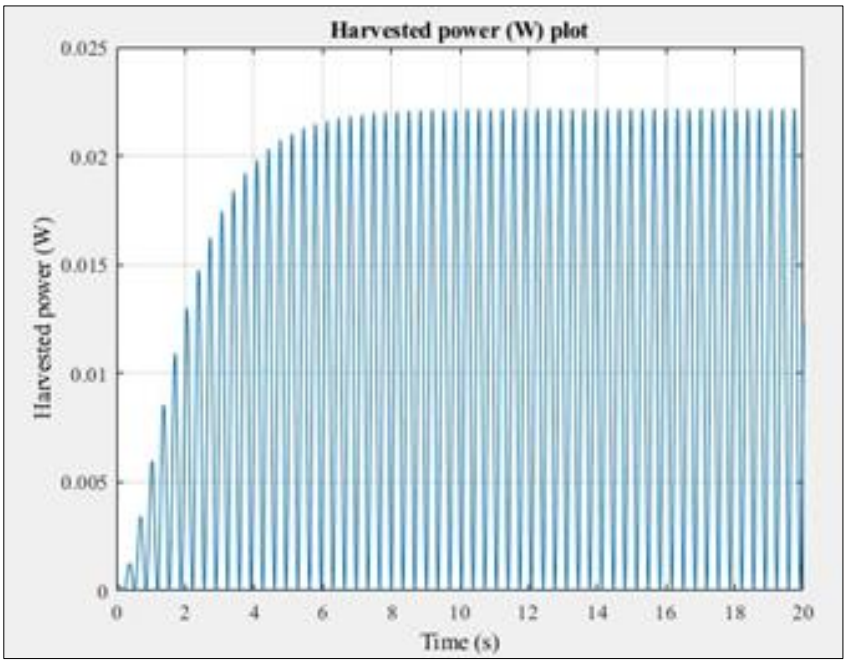

Figure 13 QCM harmonic excitation harvested power plot

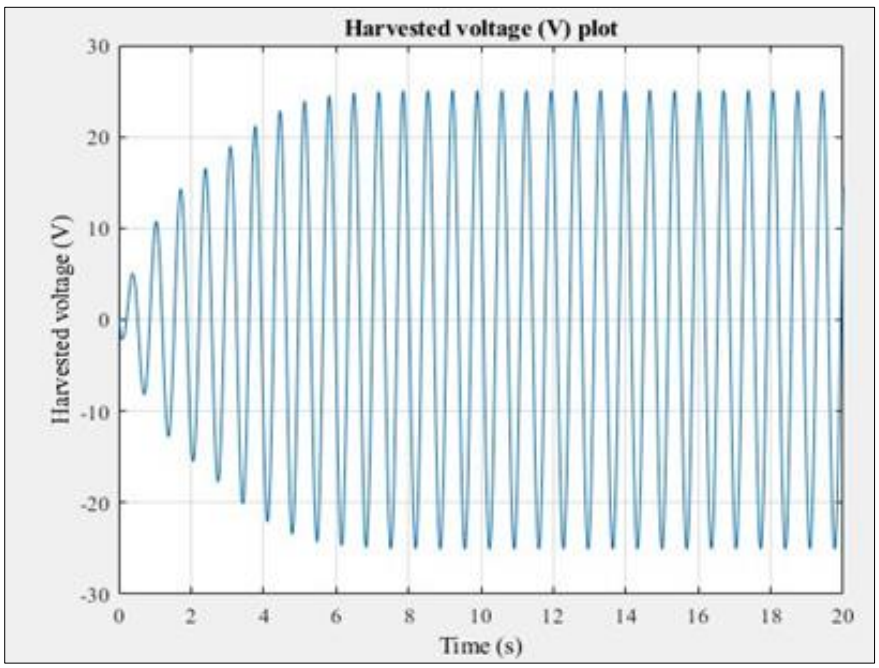

Figure 14 HCM harmonic excitation harvested voltage plot

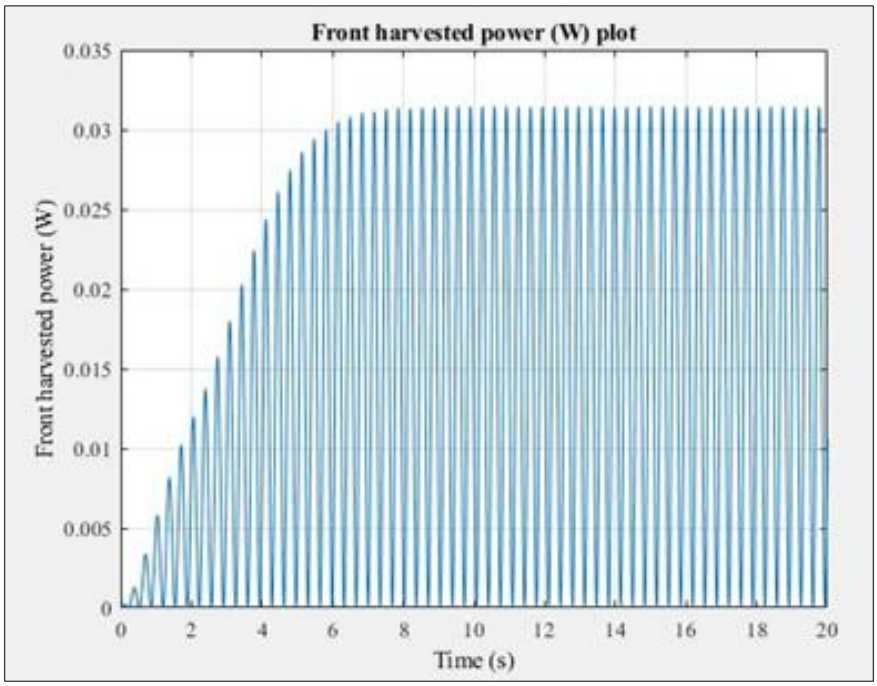

Figure 15 HCM harmonic excitation harvested power plot

The summary of the recorded peak values for the QCM and HCM are represented in Table 6 and Table 7, respectively.

Table 6 QCM harmonic excitation results

QCM	Frequency (Hz)	harvested voltage plot Peak value (V)	RMS voltage (V)	harvested power plot peak value (W)	RMS power (W)
sprung resonant frequency	1.454	20.63	14.59	0.02129	0.0007294
unsprung resonant frequency	9.529	9.606	6.79	0.004614	0.0003396

Table 7 HCM harmonic excitation results

HCM	Frequency (Hz)	Front harvested voltage plot Peak value (V)	RMS harvested voltage	Front harvested power plot peak value (W)	RMS harvested power (W)
sprung natural frequency	1.429	24.83	17.56	0.03082	0.0008779
sprung pitch natural frequency	1.004	3.138	2.22	0.004562	0.0001109
Front unsprung natural frequency	9.66	9.564	6.76	0.0004923	0.0003381
Rear unsprung natural frequency	9.66	9.564	6.76	0.004562	0.0003381

4. Conclusion

The dump truck QCM and HCM were mathematically modeled. Their equations of motion have been derived for both suspension system only and suspension system + piezoelectric stack configurations. The first configuration was used to assess the quantity of power dissipated in the frequency domain. The results revealed that the maximum power dissipated occurred at the resonant frequencies. The latter configuration was used to determine the voltage and power harvested from both the QCM and HCM. For the QCM, the maximum recorded harvested voltage is 20.63V while the

maximum harvested power is 0.02129 W. Their root mean square values are 14.59V and 0.0007294 W, respectively. For the HCM the maximum harvested voltage is 24.83 V while the maximum harvested power is 0.03082. Their root-mean-square values are 17.56 V and 0.0008779 W, respectively. The HCM results are 20.36% higher in comparison with the QCM ones. All these results revealed that the suspension system of the truck can provide sufficient power to charge batteries and power wireless sensors.

Compliance with ethical standards

Acknowledgments

I acknowledge my supervisor Pr. Dr. Erol Uzal, and my thesis committee members Prof. Dr. İbrahim Özkol and Dr. Şüle Kapkın for their continuous support throughout this research.

Disclosure of conflict of interest

The author and co-authors have no conflict of interest to declare.

References

[1] American Physical Society., Transportation and Energy Issues, 2021 [Cited 2021 Feb 19], available from: https://www.aps.org/policy/reports/energy/transportation.cfm.

[2] Use of Energy Explained, 2020 [Cited 2021 Feb 19]. available from: https://www.eia.gov/energyexplained/useofenergy/transportation.php

[3] Cao, S. and Li, J.A., 2017, Survey on ambient energy sources and harvesting methods for structural health monitoring applications, Adv. Mech. Eng., 9, 1687814017696210.

[4] Roundy, S., Wright, P.K. and Rabaey, J. A study of low-level vibrations as a power source for wireless sensor nodes. Computer Communications,2003, 26, 1131–1144.

[5] Abhijit, G., Jendrzejczyk, J., Mulcahy, M., Design of electromagnetic shock absorbers, International Journal of Mechanics and Materials in Design, 2006, 3, 285-291.

[6] Velinsky, S.A., and White, R.A., Vehicle energy dissipation due to road roughness," Veh. Syst. Dyn., 1980, 6, 359–384.

[7] Jacota, V.G., "Evaluation of the Dissipated Energy by the Automobile Dampers," Glob. J. Res. Eng., 2017, 1, 1-9.

[8] Doaa A., Tariq D. and Abdel-Hamid I.M., "A State-Of-The-Art Review of Car Suspension-Based Piezoelectric Energy Harvesting Systems", energies,2020, 13, 1–39.

[9] Wei C., and Taghavifar, H., "A novel approach to energy harvesting from vehicle suspension system: Half-vehicle model," Energy, 2017, 134, 279–288.

[10] Abdelkareem, M.A., Xu L., Ali, M.K.A., Hassan, M.A., Elagouz, A. and Zou, J., 2018, On-field measurements of the dissipated vibrational power of an SUV car traditional viscous shock absorber, ASME 2018 International Design Engineering Technical Conferences and Computers and Information in Engineering Conference.

[11] Aljadiri, R.T., Taha, L.Y., and Ivey, P., Wind energy harvesting systems: A better understanding of their sustainability, 3rd International Conference on Control, Automation and Robotics (ICCAR), 2017, 582–587.

[12] Erturk, A. and Inman, D. J., Piezoelectric Energy Harvesting, John Wiley & Sons, Ltd. ISBN: 2011, 978-0-470-68254-8

[13] Ruiz-Garcia, L., Lunadei, L., Barreiro, P. and Robla, I., A review of wireless sensor technologies and applications in agriculture and food industry: state of the art and current trends, sensors, 2009, 9(6), 4728–4750.

[14] Ipema, A.H., Goense, D., Hogewerf, P.H., Houwers, H.W.J. and Van-Roest, H., Pilot study to monitor body temperature of dairy cows with a rumen bolus, Comput. Electron. Agric., 2008, 64, 49-52.

[15] Nadimi, E.S., Sogaard, H.T., Bak, T., Oudshoorn F.W., ZigBee-based wireless sensor networks for monitoring animal and pasture time in a strip of new grass, Comput. Electron. Agric., 2008, 61, 79-87.

[16] Chen, J., Cao, X., Cheng, P., Xiao, Y. and Sun, Y., Distributed collaborative control for industrial automation with wireless sensor and actuator networks, IEEE Trans. Ind. Electron., 2010, 57(12), 4219–4230.

[17] Christin, D., Mogre, P.S. and Hollick, M., Survey on wireless sensor network technologies for industrial automation: The security and quality of service perspectives, Future Internet, 2010, 2(2), 96–125.

[18] Ko J., Lu C., Srivastava M.B., Stankovic J.A., Terzis A. and Welsh M., Wireless sensor networks for healthcare," Proc. IEEE, 2010, 98 (11), 1947–1960.

[19] Park, G., Rosing, T., Todd, M.D., Farrar, C.R. and Hodgkiss, W., Energy harvesting for structural health monitoring sensor networks, J. Infrastruct. Syst., 2008, 14(1), 64–79.

[20] García-Hernández, C.F., Ibarguengoytia-Gonzalez, P.H., García-Hernández, J. and Pérez-Díaz, J.A., "Wireless sensor networks and applications: a survey," IJCSNS Int. J. Comput. Sci. Netw. Secur., 2007, 7(3), 264–273.

[21] Liao, W.H., Wang, D.H. and Huang, S.L., 2001, Wireless monitoring of cable tension of cable-stayed bridges using PVDF piezoelectric films, J. Intell. Mater. Syst. Struct., 2001, 12(5), 331–339.